JACS
JOURNAL OF THE AMERICAN CHEMICAL SOCIETY

Article

pubs.acs.org/JACS

Photoinduced Macroscopic Morphological Transformation of an Amphiphilic Diarylethene Assembly: Reversible Dynamic Motion

Kenji Higashiguchi,*[,†,‡] Genki Taira,[†] Jun-ichiro Kitai,[†] Takashi Hirose,[†] and Kenji Matsuda*[,†]

[†]Department of Synthetic Chemistry and Biological Chemistry, Graduate School of Engineering, Kyoto University, Katsura, Nishikyo-ku, Kyoto, 615-8510, Japan

[‡]PRESTO, Japan Science and Technology Agency, Kawaguchi, 332-0012, Japan

Supporting Information

ABSTRACT: Self-assembled microstructures of an amphiphilic diarylethene featuring an alkyl chain and triethylene glycol groups showed a photoinduced reversible morphological change in water. Reversible photoisomerization of the core diarylethene gave rise to a reversible morphological transformation between colorless microspheres and colored fibers. When colorless microspheres were irradiated with UV light, colored fibers were formed, and when the colored fibers were irradiated with visible light, the spheres were restored to their original positions where the spheres originally existed. This system showed reversible morphological change through not only photoirradiation but also temperature change. These behaviors can be interpreted as a phase transition between the sphere and fiber states. The dynamic process of the phase transition was monitored by polarized optical microscopy (POM), transmission electron microscopy (TEM), and X-ray diffraction (XRD). It was revealed that the formation of fibers upon UV irradiation occurred radially at the surface of the sphere and the formation of the spheres upon visible-light irradiation occurred at the middle of the fiber. The unique photoinduced mechanical motion provides useful information for the design of sophisticated photoactuators.

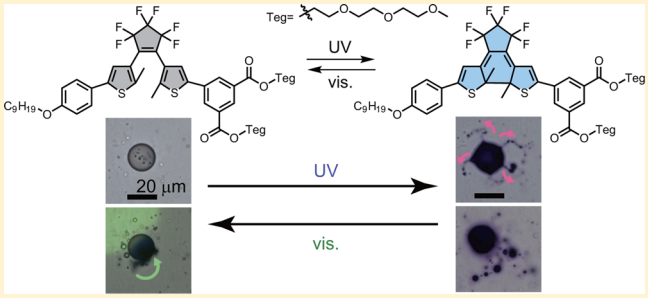

INTRODUCTION

Amphiphilic compounds form self-assembled structures such as micelles, vesicles, fibers, lamellae, and coacervates through intermolecular solvophobic interactions.[1−13] The morphology of self-assembled structure is determined by not only the molecular structure but also environmental conditions such as temperature and solvent. The control over morphology is important because the practical properties of materials depend on their morphology, when the compounds are applied to organic electronics and biomaterials.

By introducing stimuli responsiveness, a static self-assembled structure becomes dynamic when a morphological transformation takes place. Temperature change,[14−20] addition of chemicals,[21−26] sonication,[27−33] and photoirradiation[34−45] are typical examples of stimuli. Among them, photoirradiation attracts interest for its potential in practical applications, such as optoelectronics and drug delivery, because photoirradiation can be performed on a narrow area without disturbing the system.

Recently, the dynamic process of supramolecular assembly has begun to attract interest.[46−50] In particular, the dynamic process of the micro- or macroscopic morphological transformation of photoresponsive self-assembled structures attracts interest because it can convert photon energy into mechanical motion.[51−60] Finkelmann et al. and Ikeda et al. demonstrated the mechanical motion of a photoresponsive polymer through photoinduced phase transition.[51−53] Takagi et al. monitored the photoinduced morphological transformation of a lipid membrane sphere containing an azobenzene unit.[54] Feringa et al. reported the light-induced disassembly of self-assembled vesicle-capped nanotubes through a one-way photocyclization reaction of overcrowded alkenes. The one-way disassembly of fibers was monitored by epifluorescence microscopy and cryogenic transmission electron microscopy (Cryo-TEM).[59] It has been reported recently that not only supramolecular or polymer assemblies but also molecular crystals can undergo macroscopic photoinduced morphological transformation.[60,61] For a wide variety of assemblies, mechanical motion is currently under intensive investigation.

To introduce photoresponsiveness, it is important to incorporate a photoreactive moiety into the system. Azobenzenes have been frequently employed because the *cis*−*trans* geometrical change concomitant with photoisomerization is useful for the control of self-assembled structures.[34,35,51−57] Meanwhile, photochromism of diarylethenes also induces change in self-assembled structures.[36−45] While the colorless open-ring isomer has a flexible structure in solution, owing to the free rotation between the aryl groups and the ethene moiety, the colored closed-ring isomer has a rigid plate structure because of its fused-ring arrangement (Figure 1).

Received: December 19, 2014
Published: February 4, 2015

DOI: 10.1021/ja512924q
J. Am. Chem. Soc. 2015, 137, 2722−2729

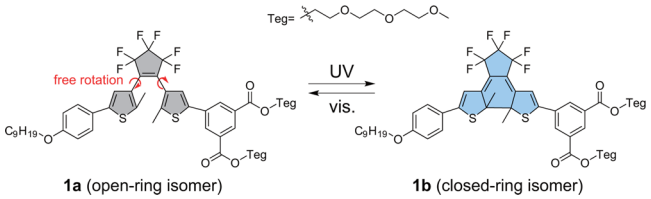

Figure 1. Photochromic reaction of amphiphilic diarylethene **1**.

Therefore, the closed-ring isomer shows stronger $\pi-\pi$ stacking than the open-ring isomer, allowing control of the self-assembled structure.

We have synthesized various amphiphilic diarylethenes with oligo(ethylene glycol) side chains and reported the photo-induced change in the supramolecular assembly; exciton-coupled circular dichroism and lower critical solution temperature were photochemically controlled.[44,45] These works focused mainly on photoswitching behavior, so dynamics of morphological transformation was not monitored.

In this paper, we report the reversible morphological transformation between colorless microspheres and colored fibers concomitant with the photochromism of diarylethenes. The dynamic morphological transformation of a microsphere monitored by optical microscopy, TEM, and X-ray diffraction (XRD) will be reported in detail. When the colorless microspheres are irradiated with UV light, colored fibers are formed, which, upon irradiation with visible light, revert to microspheres in their original positions.

RESULTS AND DISCUSSION

Molecular Design and Synthesis. In this study, we designed amphiphilic diarylethene **1** with an asymmetric structure: one side has a nonyloxy chain as the hydrophobic group, and the other side has two triethylene glycol units as the hydrophilic group (Figure 1). The core moiety, 1,2-bis(2-methyl-5-phenyl-3-thienyl)hexafluorocyclopentene,[62] is known to exhibit a high conversion ratio from the open-ring to the closed-ring isomer upon irradiation with UV light (97% in the photostationary state (PSS) upon irradiation with 313 nm light in hexane). The conversion is determined by the ratio of the product of the absorption coefficient and the cyclization or cycloreversion quantum yield, as shown in eq 1.[63] The high conversion is attributed to the low quantum yield of the cycloreversion reaction ($\Phi_{c\to o}$) of 1,2-bis(2-methyl-5-phenyl-3-thienyl)hexafluorocyclopentene.

$$\text{conversion} = \frac{\varepsilon_o \Phi_{o\to c}}{\varepsilon_o \Phi_{o\to c} + \varepsilon_c \Phi_{c\to o}} \quad (1)$$

Amphiphilic diarylethene **1** was synthesized using 1,2-bis(2-methyl-3-thienyl)hexafluorocyclopentene,[64] which is a non-substituted diarylethene at the 5-position of thiophene ring, as an intermediate. Direct C−H arylation at the 5-position of the thiophene ring was the key reaction.[65] The intermediate diarylethene and iodobenzenes featuring hydrophobic and hydrophilic groups were heated at reflux in *m*-xylene along with 2,2′-bipyridine, palladium(II) chloride, and silver(I) carbonate. The detailed synthetic procedure is described in the Supporting Information. The structure of amphiphilic diarylethene **1a** was confirmed by NMR spectroscopy and mass spectrometry.

Photochromic Reaction in Acetonitrile and Water. Photochromic properties of diarylethene **1** were measured in acetonitrile, as shown in Figure 2a. Diarylethene **1** showed

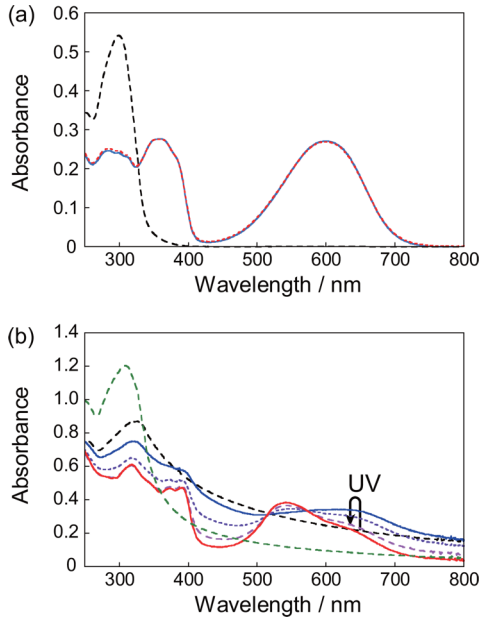

Figure 2. Spectral change of **1** induced by photoirradiation. (a) Absorption spectra of open-ring isomer **1a** (black broken line), closed-ring isomer **1b** (blue solid line), and at the photostationary state (PSS) upon irradiation with 313 nm light (red dotted line) in acetonitrile. The conversion was 99% at the PSS. The absorption maximum of **1b** was at 598 nm in the visible range. (b) Change in absorption spectra upon irradiation with UV light in aqueous suspension: before irradiation (black broken line), after 2 min (blue solid line), 10 min (violet dotted line), 30 min (purple broken line), and 60 min (red solid line) of irradiation. Green broken line denotes the spectrum after subsequent irradiation with visible light for 30 min. The absorption maximum at the PSS was at ≈540 nm.

excellent photochromic performance; the conversion ratio of the open-ring (**1a**) to the closed-ring isomer (**1b**) was 1:99 at the PSS upon irradiation with 313 nm light. The colorless isomer, **1a**, had no absorption band in the visible range, whereas the colored isomer, **1b**, showed a blue color with an absorption maximum at 598 nm. The color disappeared upon irradiation with 578 nm light.

Amphiphilic diarylethene **1** was not soluble in water upon direct addition; therefore, the aqueous solution was prepared through the addition of a large excess of water (4 mL) to a small amount of the acetonitrile solution (0.5 mL) and subsequent 10-fold dilution with water at room temperature, upon which open-ring isomer **1a** formed a suspension in water (see Supporting Information). The photochromic behavior of this suspension was different from that in the acetonitrile solution. In the initial state, the scattering due to the formation of aggregates of open-ring isomer **1a** raised the baseline up to 800 nm, as shown in Figure 2b. Upon irradiation with UV light, the absorbance around 650 nm increased initially, but began to decrease with further UV irradiation. Finally, a new band appeared around 540 nm and the band around 650 nm remained as a shoulder. The decrease in scattering around 800 nm indicated that the size of the scattering particles decreased upon isomerization to the closed-ring isomer. Upon subsequent irradiation with visible light, the absorption band around 540 nm disappeared, but the baseline was not restored completely. This indicates that the size of the scattering particle in the suspension of open-ring isomer **1a** is not always the same.

DOI: 10.1021/ja512924q
J. Am. Chem. Soc. 2015, 137, 2722−2729

Photoinduced Morphological Change of Microstructures. The suspension was found to consist of a few micrometer-sized spheres, as observed under an optical microscope using transmitted light illumination (Figure 3a).

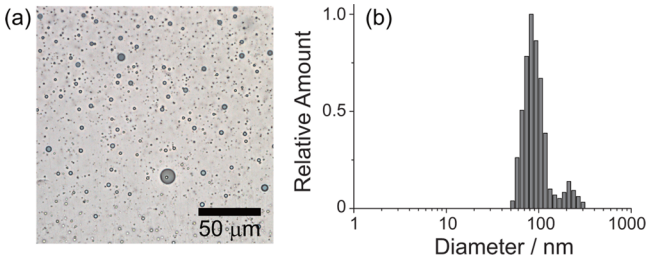

Figure 3. (a) Optical image of the suspension in water at room temperature of open-ring isomer **1a**. Volume-weighted size distribution of the particles measured by DLS.

The formation of the submicrometer-sized spheres (ca. 100 nm) was also confirmed by dynamic light scattering (DLS) measurement (Figure 3b). Transmission electron microscopy (TEM) also supports the size distribution (Supporting Information Figure S14a). Upon irradiation with UV and visible light, photoinduced change of the DLS was observed (Supporting Information Figure S4).

Photoirradiation with UV and visible light was performed using focused light from a low-output mercury lamp under an epi-illumination system at 15 °C and the morphological change was monitored (Figure 4a and Movie S1). The micrometer-sized spheres turned blue upon irradiation with UV light, and after 1 min of continuous UV irradiation, the boundaries of the spheres became obscure. Upon further irradiation, division of the microsphere was observed, with smaller spheres separating from the larger ones. A red-purple hazy fringe was discerned around the spheres. In addition, Brownian motion of the small spheres was suppressed after UV irradiation. When the sample was kept in the dark for 24 h without photoirradiation, the morphological change was not observed. We also confirmed that evaporation of the solvent does not induce the observed morphological change (Supporting Information Figure S11).

Subsequent irradiation with visible light was carried out under the epi-illumination system (Figure 4b and Movie S1). The widely diffused small spheres converged to their original positions. The diffused red-purple hazy fringe shrank like rubber and colorless spheres were restored at their initial positions. Notably, even remote spheres converged because of this shrinking of the hazy fringe. The Brownian motion of the small spheres was reactivated. This result indicated that the hazy fringe consisted of fiber structures that prevented the Brownian motion. Another example of the division and convergence is shown in Figure 4c,d (Movies S2 and S3). In this case, UV irradiation was carried out for a long period and the microspheres are widely dispersed, disrupting the connection of fibers. Therefore, convergence was not complete upon irradiation with visible light. The suppression and reactivation of the Brownian motion of small spheres were also observed.

The photoinduced transformation showed a different response to temperature. The above photoinduced transformation was observed at 15 °C, but was not observed at higher temperatures. At 40 °C, the colorless microspheres showed only photochromism upon irradiation with UV and visible light; the morphological change was not observed

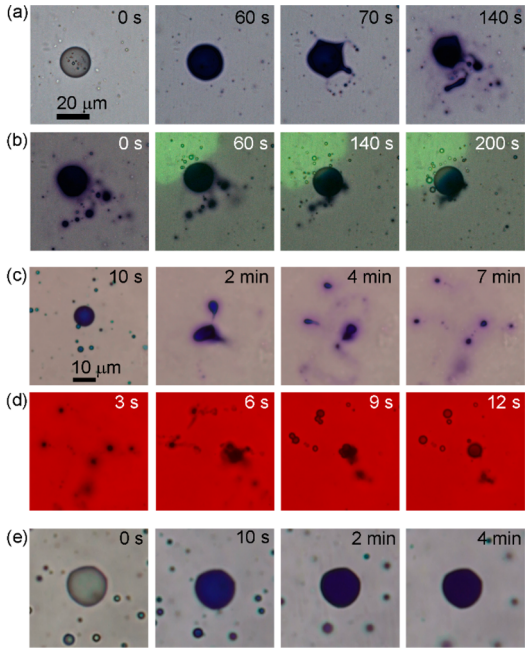

Figure 4. Photoinduced macroscopic morphological transformation of the supramolecular assemblies of **1**. (a) Division of a microsphere induced by UV irradiation. (b) Convergence to the original microsphere upon subsequent irradiation with visible light (see Movie S1). (c) Division of a microsphere induced by UV irradiation (see Movie S2). (d) Convergence to the original microsphere upon subsequent irradiation with visible light (see Movie S3). (e) UV irradiation of microsphere at 40 °C. Photochromic reaction was induced, but the morphological change did not occur. These optical microscope observations in water were performed in transmission geometry using an objective lens (40×/0.75). A glass cell was filled with an aqueous suspension and observed before evaporation. The effect of drying on the morphology was discussed in Supporting Information Figure S11. The irradiation with UV (365 nm) and visible (green, 546 nm) light was carried out using a mercury lamp and some optical filters. The irradiation powers of UV (a) and visible (b) light were 6.2 and 25 mW/cm^2, respectively (Supporting Information Figure S2). The red background color of (d) was due to the filters used to remove strong green light.

(Figure 4e). At 20 and 25 °C, the spheres did not undergo division; however, the red-purple fibers were generated (Supporting Information Figure S5). The division was suppressed at higher temperatures. The suppression at high temperature indicates that the morphological change is ascribed to the photoisomerization and not to the photothermal effect that is caused by local rise in temperature.[46]

A Maltese cross pattern was observed for the UV-irradiated microsphere possessing a red-purple region in the polarized optical microscopy (POM) image under the cross-Nicol condition (Figure 5). The transmittance of a birefringent sample depends on $\sin^2 2\theta$, where θ is the angle between the polarizer and the optical axis of the anisotropic sample. When the samples have spherocrystal structures, which are radially symmetric arrays and whose optical axes also align radially, a dark cross appears at $\theta = 0°$ and 90°.[66] The POM result suggests that the fibers formed radially from the microsphere like a spherocrystal. Although the hazy red-purple region showed a Maltese cross pattern, colorless and colored microspheres did not transmit light under the cross-Nicol condition, suggesting that the microspheres did not form spherocrystal structures.

DOI: 10.1021/ja512924q
J. Am. Chem. Soc. 2015, 137, 2722−2729

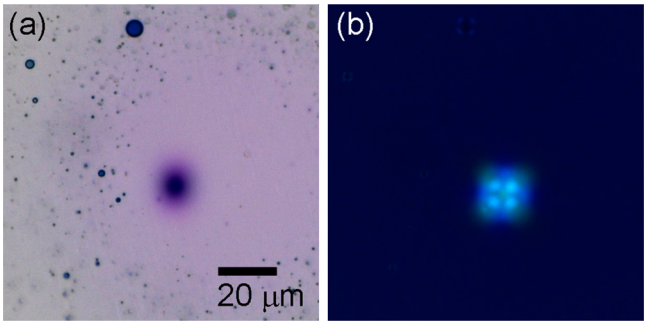

Figure 5. POM images under (a) para-Nicol and (b) cross-Nicol conditions. The UV-irradiated microsphere showed a Maltese cross pattern because of the radial structure of the fiber-like aggregates.

Thermally Induced Morphological and Spectral Changes of Microstructures. A morphological change also occurred because of a temperature stimulus. The colorless microspheres of **1a** did not show transformations upon cooling from 40 to 5 °C. In contrast, the colored microspheres that were UV-irradiated at 40 °C divided into small particles upon cooling to 5 °C (Figure 6a and Movie S4). In this case, small

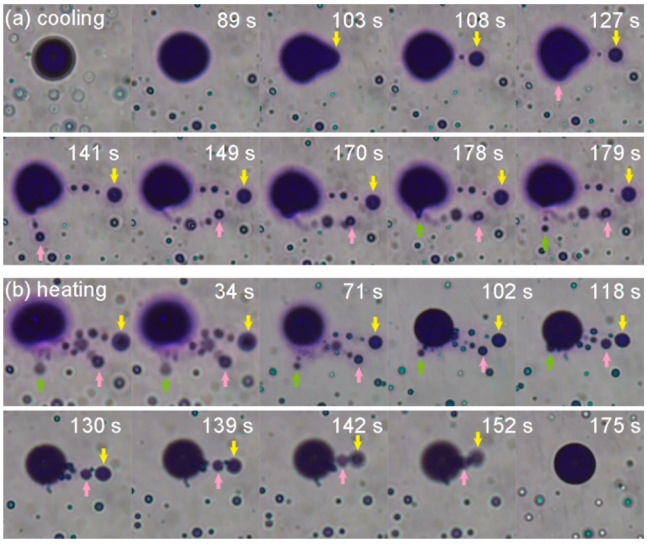

Figure 6. Morphological change of a well-colored microsphere, which was mainly composed of closed-ring isomer **1b**, caused by (a) fast cooling from 40 to 5 °C (see Movie S4) and (b) subsequent fast heating from 5 to 40 °C (see Movie S5). The temperature control was carried out using a Peltier stage.

spheres were squeezed out sequentially like a bead necklace, and a red-purple region was also generated. Both the "necklace" particles and the red-purple region converged into the main sphere upon subsequent heating to 40 °C (Figure 6b and Movie S5).

The temperature stimulus affected the aggregates not only on the surface but also in the inner region. This means that the morphological change of the aggregates occurred homogeneously; therefore, the division presumably occurred gently and the bundles of fibers connecting the separated spheres were not disrupted. Therefore, in this thermally induced change, the convergence of the separated microspheres occurred completely.

Changes in absorption spectra concomitant with the thermal morphological changes were investigated. Initially, the aqueous suspension was irradiated with UV light and the ratio of the open-ring to the closed-ring isomer was determined by HPLC. Then, the spectral change of the sample containing 95% of the closed-ring isomer was measured under cooling in aqueous media (Figure 7a). From 50 to 40 °C, the shape of the

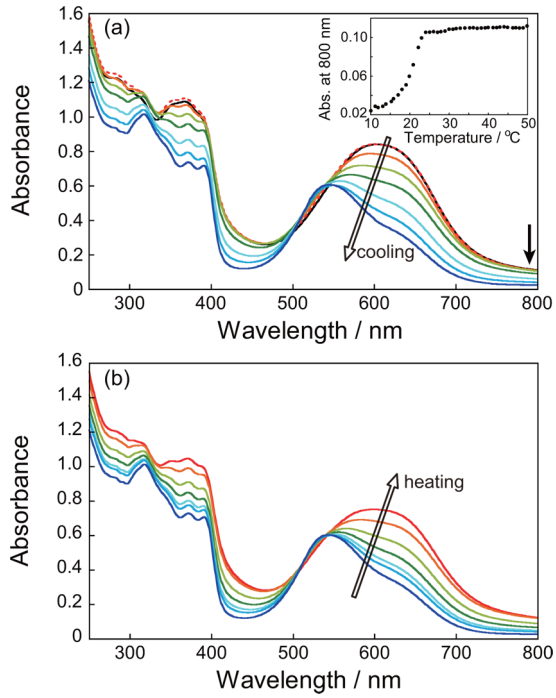

Figure 7. (a) The change in the absorption spectrum upon cooling from 50 to 10 °C. Spectra were obtained at 50 °C (black), 40 °C (dotted red), 30 °C (orange), 26 °C (yellowish green), 22 °C (green), 20 °C (sky blue), 17 °C (blue), and 10 °C (dark blue). The aqueous suspension contained 5% **1a** and 95% **1b**. Inset shows the turbidity change upon cooling monitored through the absorbance at 800 nm (black arrow). The temperature of the clearing point was 23 °C. (b) The change in absorption spectra caused by heating from 10 to 40 °C. Spectra were obtained at 10 °C (dark blue), 17 °C (blue), 20 °C (sky blue), 23 °C (green), 26 °C (yellowish green), 30 °C (orange), and 40 °C (red).

absorption band around 600 nm was similar to that in the acetonitrile solution. In contrast, a new band began to appear at a shorter wavelength around 540 nm below 30 °C and became more distinct with cooling. The blue shift is consistent with the color of the aggregates; the sphere is blue and the fiber is red-purple. The reversible spectral change occurred upon subsequent heating (Figure 7b). The inset of Figure 7a shows the temperature dependence of scattering monitored at 800 nm, where both isomers had no absorption.[67] The temperature of the clearing point was 23 °C for the aggregates containing 95% of closed-ring isomer **1b**. The clearing point was dependent on the ratio of the isomers (Supporting Information Figure S10).

The spectrum at 10 °C (Figure 7, dark blue line) is similar to the UV-irradiated spectrum at room temperature (Figure 2b, red line), suggesting that the photogenerated and thermogenerated fiber states are identical. In the sphere state at high temperature, the absorption spectrum is similar to that in organic solvent, whereas in the fiber state at low temperature, a blue-shifted structured absorption spectrum was observed. This means that the diarylethene molecules are molecularly

DOI: 10.1021/ja512924q
J. Am. Chem. Soc. 2015, 137, 2722−2729

dispersed in the sphere state, but significant intermolecular interactions operate in the fiber state, which is composed of entangled fibers made of the stacked diarylethene molecules. The absorption spectrum showed a blue shift from a broad band at 600 nm in the sphere state to a relatively narrow band at 540 nm in the fiber state, suggesting the formation of H-aggregates in the fiber state.[68,69] It was believed that the closed-ring isomers are regularly packed parallel to one another, and construct ordered supramolecular structures in the fiber state. Therefore, by raising the temperature, thermal agitation overcomes the intermolecular interactions and prevents the formation of ordered structures. This is considered to be the reason no fiber formation was observed upon UV irradiation at high temperature.

Investigation of the Structure of the Assembly. In order to obtain information on the structure of the assemblies, TEM images were obtained for samples under various conditions. The supramolecular assemblies at various conversion ratios showed several nanostructures under negative staining, as shown in Figure 8a–d. The microspheres of the

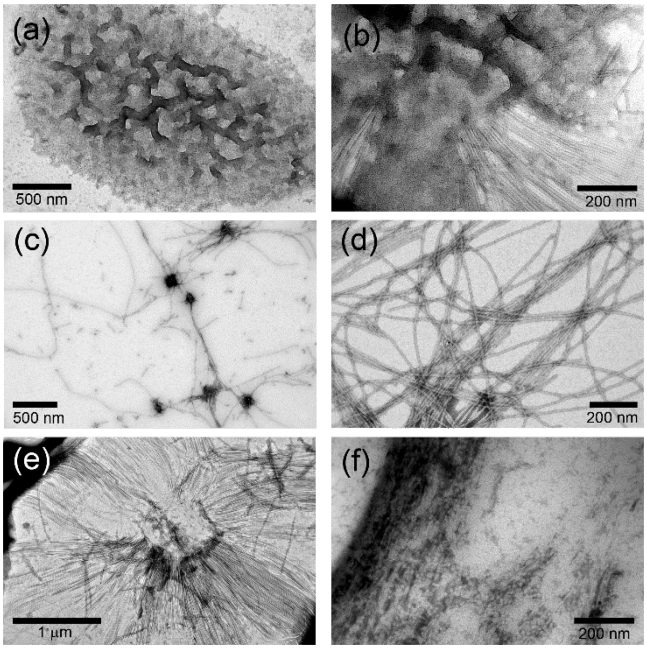

Figure 8. TEM images of supramolecular assemblies. TEM was performed using negative staining by sodium phosphotungstate. The conversion ratios of closed-ring isomer **1b** were (a) 0% (open-ring isomer **1a**), (b) 48%, (c) 64%, and (d) 100% (closed-ring isomer **1b**). (e) TEM image of microspheres after UV irradiation on the TEM grid. The generation of the fibers from the spheres is observed. (f) TEM image of fibers after visible-light irradiation on the TEM grid. The generation of the spheres from the fibers is observed.

open-ring isomer were not completely filled structures like oil droplets, but coacervate structures with a cocontinuous morphology suggested by the included aqueous phase of the stained moiety (Figure 8a).[70,71] The negatively stained water phase inside the microsphere adopted a sponge-like branching morphology. On the other hand, the closed-ring isomer formed fibers with a uniform diameter (8.2 ± 0.5 nm) without branched structures (Figure 8d).

At the intermediate conversion ratio, the microspheres and fibers coexisted. At a conversion ratio of 17%, microspheres with the cocontinuous morphology were observed, as in the case of the open-ring isomer (Supporting Information Figure S14c). At a conversion ratio of 48%, a branched network structure of fibers was observed, and there were nodes where the fibers gathered (Figure 8b). The diameter of the fibers was equal to that observed for the closed-ring isomer. The structure of the node was similar to those of the microspheres composed of the open-ring isomer. In the node, the water phase adopted a sponge-like branching morphology (Supporting Information Figure S14d). At 64% conversion, the branched network structure was also observed, but the nodes were much smaller than in the case of 48% conversion (Figure 8c). In this case, the node was spherical, but the structure inside the node appeared to consist of short fibers (Supporting Information Figure S14g). The diameters of the fibers at 48 and 64% conversion were 8.6 ± 1.0 and 9.3 ± 0.9 nm, respectively.

To obtain information on the dynamic process of the transition from sphere to fiber states, microspheres were placed on a TEM grid and TEM images were obtained after UV irradiation (Figure 8e). The image shows the radial generation of fibers with a vacancy at the center. The phase transition from microspheres to fibers was caused by the increase in the conversion ratio on the surface of the microsphere. The starting material of the microsphere was used up after prolonged UV irradiation, and a vacancy was considered to be formed. This radial generation of fibers is consistent with the observation of the Maltese cross in the POM image.

Then, to obtain information on the transition from fiber to sphere states, fibers were placed on a TEM grid and TEM images were obtained after visible-light irradiation (Figure 8f). In the image after visible-light irradiation, the bundle of fibers was also observed like in the image before irradiation, but fragmentation and deformation of the fiber was discerned. Between the fragments, a granular texture was observed and the edge line of the fibers became obscure. This image is considered to represent the initial stage of the transformation from fiber to sphere state.

Figure 8e,f are the "snapshot" during the photoinduced phase transition. Because the photoirradiation of the aqueous suspension was carried out on the TEM grid, monitoring the photoinduced morphological transformation was possible using TEM. These images reveal the structure during photoirradiation.

Small-angle X-ray diffraction measurements were performed on the sample with >95% **1b** in water (Figure 9a,b). It is known that axially symmetric fibers usually bundle with hexagonal packing.[72] The obtained *d*-spacing values of obvious peaks were 12, 6.5, 5.1, and 3.3 nm and these diffraction peaks were indexed as (100), (110), (200), and (220) of hexagonal packing ($a/2 = d_{(110)} = 6.5$ nm), respectively. The diameter of the fiber was 6.5 nm, which is consistent with the diameters measured from the TEM image (8.2 nm), which may be flattened by adhering on substrate. MM/MD simulation also showed rod-like micelle structures with diameters of ca. 8 nm that consist of ca. 20 molecules in one turn (Figure 10). The diffraction pattern appeared in the perpendicular direction of shear, suggesting the alignment of the fibers upon shearing. The diffraction measurements were also performed on mixtures with various conversion ratios using synchrotron radiation (Supporting Information Figure S13). The diffraction patterns appeared at high conversion ratios (88%), whereas no diffraction was observed in the case of low conversion ratios. These results also showed that fibers were formed at high conversion ratios.

DOI: 10.1021/ja512924q
J. Am. Chem. Soc. 2015, 137, 2722–2729

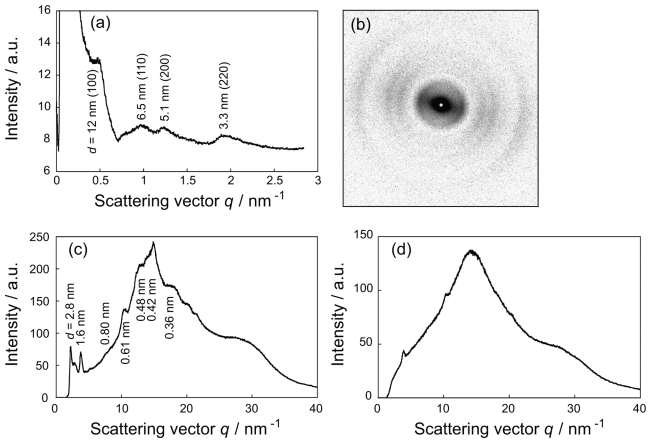

Figure 9. (a) Small-angle XRD pattern of >95% **1b** in the hydrated paste. (b) The diffraction image of fibers stretched by the shear stress along the up−down direction. Wide-angle XRD pattern of >95% **1b** in the (c) hydrated and (d) dehydrated paste.

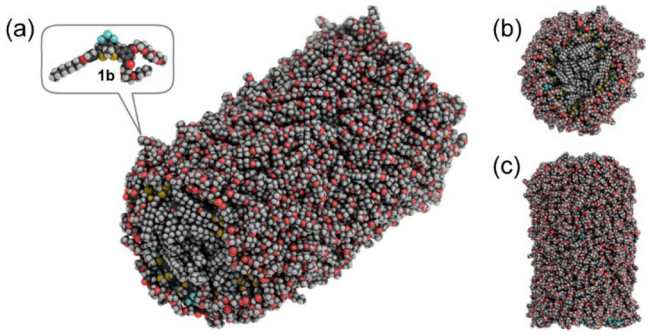

Figure 10. (a) The MM/MD-simulated fiber structure composed of **1b**. (b) Top view and (c) side view. The diameter was ca. 8 nm.

Wide-angle X-ray diffraction measurement was also performed (Figure 9c). The diffraction peak at ca. q = 17.5 nm^{-1} (0.36 nm) was assigned to $\pi-\pi$ stacking of the closed-ring isomers. Other diffraction peaks indicate that the molecules of **1b** had ordering not only in the face-to-face direction but also in other directions. It is hypothesized that two molecules packed in the head-to-head manner to avoid steric hindrance caused by the out-of-plane methyl groups and the perfluorocyclopentene moieties. Amorphous halo, which is caused by the disordered packing of the neighboring molecules, was also observed around q = 14 nm^{-1} (0.44 nm) as background. After evaporation of the solvent water, only the halo was observed (Figure 9d). This halo was observed also for the open-ring isomer in water, which forms microsphere structure (Supporting Information Figure S12). These results suggest that red-purple fibers having H-aggregate stacking structure required hydration of hydrophilic moiety. The evaporation caused dehydration of triethylene glycol and the orientation of molecules of the closed-ring isomer became random. The evaporation of the solvent water from the hydrated assembly of the closed-ring isomer **1b** also caused the color change from red−purple to blue, which also indicates disassembly of the fiber structure (Supporting Information Figure S11b).

Mechanism of Morphology Transition. The phase diagram of the self-assembled amphiphilic compound has been of interest. For example, a lyotropic liquid crystal consisting of a monoglyceride and water was reported to form a bicontinuous cubic phase at a higher temperature and lamella phase at a lower temperature.[73,74] In our case, similar behavior of phase transition between coacervate and fiber phases was observed from the temperature change and from the photochemical isomerization of the component.

Remarkably, the effect of lowering the temperature is equivalent to the effect of raising the ratio of the closed-ring isomer; therefore, the fiber-state formation was observed either upon irradiation with UV light isothermally or upon cooling the blue-colored aggregates. The photo- and thermo-induced morphological transformation can be interpreted by considering the phase transition between the sphere and the fiber states (Figure 11a,b), which is defined by the temperature and the ratio of the components.

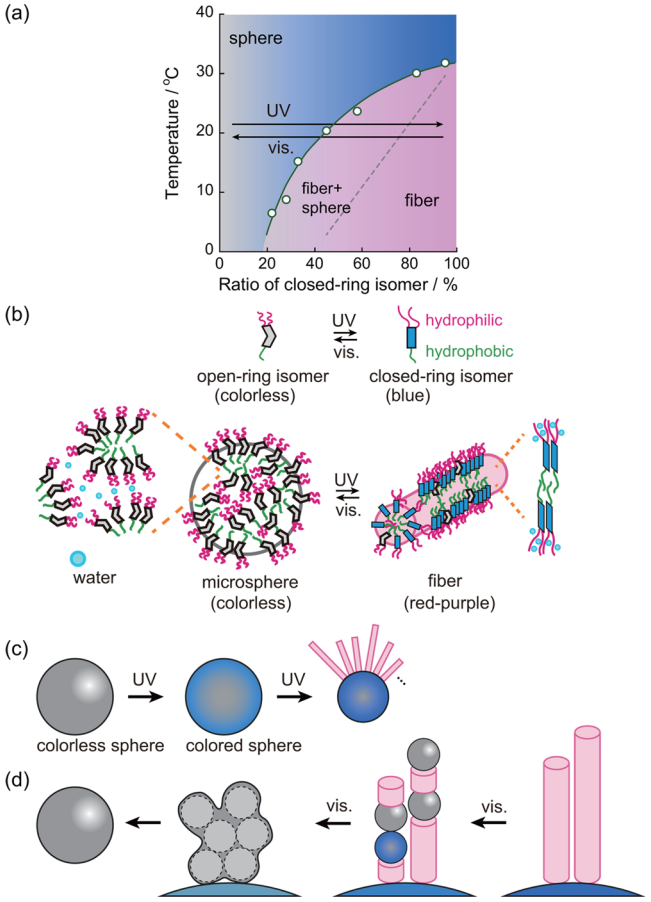

Figure 11. (a) Phase diagram of the mixture of **1a** and **1b**. The transition temperatures were obtained from the turbidity change upon cooling (green open circle). Data are taken from the inset of Figure 7a and Supporting Information Figure S10. (b) Schematic illustration of the photoinduced morphological transformation of the supramolecular assembly. (c) Schematic illustration of the dynamic process of the phase transition from sphere to fiber states and (d) from fiber to sphere states.

When the UV-irradiated red-purple substance was dried, the color changed to blue (Supporting Information Figure S11b). This result suggests that the red-purple substance contains water. The UV-generated fiber state is the low-temperature phase and the original sphere state is the high-temperature phase. Therefore, taking into account the entropic effects, the sphere state has higher entropy than the fiber state does. It is suggested that the fiber state has a hydrogen-bonded hydrated structure and the sphere state has a phase-separated structure.

DOI: 10.1021/ja512924q
J. Am. Chem. Soc. 2015, 137, 2722−2729

The transition is considered to occur between the hydrated and the dehydrated structures similarly to the LCST behavior often observed in oligo(ethylene glycol) derivatives.[45,75] The sphere state showed a phase-separated coacervate structure in its TEM image. The closed-ring isomer has rigid planar structure, so that the aggregated fiber structure is considered to be preferable.

Figure 11c,d show the plausible mechanism of the morphological transformation induced by photoirradiation, which were suggested by the above measurements (POM, TEM, XRD, and changes in the absorption spectra). Because the photoreaction proceeds preferentially near the surface of the aggregates owing to the absorption of light, the phase transition from the sphere to the fiber occurred on the microsphere surfaces. Thus, a red-purple region formed around the microspheres as a spherocrystal. The local heterogeneity of absorption is believed to induce the deformation and vigorous division of the sphere. As discussed above, thermally induced morphological changes show more gentle division and more complete convergence than do the light-induced changes, possibly because the temperature stimulus affected the substance homogeneously.

In the case of the restoration of microspheres, the transition occurs from the fibers. Initially, the nanospheres formed at the middle of the fibers, resulting in the subsequent shrinking of the fibers. Then, the convergence of the separated microspheres occurred through the shrinking of fibers between the spheres. After prolonged UV irradiation, the microspheres were no longer connected by fibers, so the convergence of the microspheres could not occur.

CONCLUSIONS

In conclusion, we have designed and synthesized amphiphilic diarylethene **1**, which formed a supramolecular assembly in water. A reversible morphological transformation between the microspheres and fibers was observed along with the photochromic reaction. This transformation of the supramolecular structures was also observed upon changing the temperature. These behaviors can be interpreted by considering the phase transition between the sphere and fiber states. The dynamic process of the phase transition was monitored by POM, TEM, and XRD. It was revealed that the formation of fibers upon UV irradiation occurred radially at the surface of the sphere and the formation of spheres upon visible-light irradiation occurred at the middle of the fiber. The unique photoinduced mechanical motion provides useful information for the design of sophisticated photoactuators.

ASSOCIATED CONTENT

Supporting Information

Experimental details, ^{1}H and ^{13}C NMR spectra, additional figures, and movies. Movie S1. Photoinduced macroscopic morphological transformation of the supramolecular assemblies. Division of microsphere induced by UV irradiation and convergence to the original microsphere upon subsequent irradiation with visible light (see Figure 4a,b). The movie has a 360 × 270 μm field of view for 620 s at a frame rate of 10 s/frame by 100-fold speed of reproduction. Movie S2. Division of microsphere induced by UV irradiation (see Figure 4c). The movie has a 160 × 90 μm field of view for 380 s at a frame rate of ∼4.3 s/frame by 128-fold speed of reproduction. Movie S3. Convergence to the original microsphere upon subsequent irradiation with visible light to the divided sample (see Figure 4d). The movie has a 160 × 90 μm field of view for 16 s at a frame rate of ∼0.13 s/frame by 4-fold speed of reproduction. Movie S4. Thermally induced morphological change of a well-colored microsphere caused by fast cooling from 40 to 5 °C (see Figure 6a). The movie has a 160 × 90 μm field of view for ca. 160 s at a frame rate of ∼1.1 s/frame by 32-fold speed of reproduction. Movie S5. Thermally induced morphological change by subsequent fast heating from 5 to 40 °C to the divided sample (see Figure 6b). The movie has a 160 × 90 μm field of view for ca. 140 s at a frame rate of ∼1.1 s/frame by 32-fold speed of reproduction. This material is available free of charge via the Internet at http://pubs.acs.org.

AUTHOR INFORMATION

Corresponding Authors

higashi@sbchem.kyoto-u.ac.jp
kmatsuda@sbchem.kyoto-u.ac.jp

Notes

The authors declare no competing financial interest.

ACKNOWLEDGMENTS

This work was supported by PRESTO, JST; the NEXT program, JSPS (No. GR062); and a Grant-in-Aid for Scientific Research on Innovative Areas "Photosynergetics" (No. 26107008) from MEXT, Japan. We thank Rigaku Corp., Osaka Branch for the wide-angle X-ray diffraction measurements. The synchrotron XRD measurement was performed under the approval of the Photon Factory Program Advisory Committee (Proposal No. 2012G747) and we thank Prof. Y. Kageyama (Hokkaido Univ., Japan) for the XRD measurements.

REFERENCES

(1) Matson, J. B.; Stupp, S. I. *Chem. Commun.* **2012**, *48*, 26−33.
(2) Stupp, S. I.; Palmer, L. C. *Chem. Mater.* **2014**, *26*, 507−518.
(3) Kim, H.-J.; Kim, T.; Lee, M. *Acc. Chem. Res.* **2011**, *44*, 72−82.
(4) Ryu, J.-H.; Hong, D.-J.; Lee, M. *Chem. Commun.* **2008**, 1043−1054.
(5) Lee, M.; Cho, B.-K.; Zin, W.-C. *Chem. Rev.* **2001**, *101*, 3869−3892.
(6) Shimizu, T.; Masuda, M.; Minamikata, H. *Chem. Rev.* **2005**, *105*, 1401−1443.
(7) Rosen, B. M.; Wilson, C. J.; Wilson, D. A.; Peterca, M.; Iman, M. R.; Percec, V. *Chem. Rev.* **2009**, *109*, 6275−6540.
(8) Ky Hirschberg, J. H. K.; Brunsveld, L.; Ramzi, A.; Vekemans, J. A. J. M.; Sijbesma, R. P.; Meijer, E. W. *Nature* **2000**, *407*, 167−170.
(9) Hill, J. P.; Jin, W.; Kosaka, A.; Fukushima, T.; Ichihara, H.; Shimomura, T.; Ito, K.; Hashizume, T.; Ishii, N.; Aida, T. *Science* **2004**, *304*, 1481−1483.
(10) Zhang, X.; Rehm, S.; Safont-Sempere, M. M.; Würthner, F. *Nat. Chem.* **2009**, *1*, 623−629.
(11) Görl, D.; Zhang, X.; Würthner, F. *Angew. Chem., Int. Ed.* **2012**, *51*, 6328−6348.
(12) Rybtchinski, B. *ACS Nano* **2011**, *5*, 6791−6818.
(13) Mayoral, M. J.; Fernández, G. *Chem. Sci.* **2012**, *3*, 1395−1398.
(14) Aathimanikandan, S. V.; Savariar, E. N.; Thayumanavan, S. *J. Am. Chem. Soc.* **2005**, *127*, 14922−14929.
(15) Chang, D. W.; Dai, L. *J. Mater. Chem.* **2007**, *17*, 364−371.
(16) Lee, E.; Jeong, Y.-H.; Kim, J.-K.; Lee, M. *Macromolecules* **2007**, *40*, 8355−8360.
(17) Hayashi, H.; Ohkubo, K.; Karasawa, S.; Koga, N. *Langmuir* **2011**, *27*, 12709−12719.
(18) Das, A.; Ghosh, S. *Angew. Chem., Int. Ed.* **2014**, *53*, 1092−1097.
(19) Kashyap, S.; Jayakannan, M. *J. Mater. Chem. B* **2014**, *2*, 4142−4152.

DOI: 10.1021/ja512924q
J. Am. Chem. Soc. 2015, 137, 2722−2729

(20) Wang, L.; Zou, H.; Dong, Z.; Zhou, L.; Li, J.; Luo, Q.; Zhu, J.; Xu, J.; Liu, J. *Langmuir* **2014**, *30*, 4013−4018.
(21) Park, K. H.; Lee, J.-S.; Park, H.; Oh, E.-H.; Kim, J.-M. *Chem. Commun.* **2007**, 410−412.
(22) Zhang, W.; Jin, W.; Fukushima, T.; Ishii, N.; Aida, T. *Angew. Chem., Int. Ed.* **2009**, *48*, 4747−4750.
(23) Golubkov, G.; Weissman, H.; Shirman, E.; Wolf, S. G.; Pinkas, I.; Rybtchinski, B. *Angew. Chem., Int. Ed.* **2009**, *48*, 926−930.
(24) Zhang, K.-D.; Wang, G.-T.; Zhao, X.; Jiang, X.-K.; Li, Z.-T. *Langmuir* **2010**, *26*, 6878−6882.
(25) Kim, H.-J.; Kang, S.-K.; Lee, Y.-K.; Seok, C.; Lee, J.-K.; Zin, W.-C.; Lee, M. *Angew. Chem., Int. Ed.* **2010**, *49*, 8471−8475.
(26) Hsu, W.; Chen, Y.-L.; Horng, J.-C. *Langmuir* **2012**, *28*, 3194−3199.
(27) Naota, T.; Koori, H. *J. Am. Chem. Soc.* **2005**, *127*, 9324−9325.
(28) Wang, C.; Zhang, D.; Zhu, D. *J. Am. Chem. Soc.* **2005**, *127*, 16372−16373.
(29) Isozaki, K.; Takaya, H.; Naota, T. *J. Am. Chem. Soc.* **2007**, *46*, 2855−2857.
(30) Wang, Y.; Zhan, C.; Fu, H.; Li, X.; Sheng, X.; Zhao, Y.; Xiao, D.; Ma, Y.; Ma, J. S.; Yao, J. *Langmuir* **2008**, *24*, 7635−7638.
(31) Yu, X.; Liu, Q.; Wu, J.; Zhang, M.; Cao, X.; Zhang, S.; Wang, Q.; Chen, L.; Yi, T. *Chem.—Eur. J.* **2010**, *16*, 9099−9106.
(32) Ke, D.; Zhan, C.; Li, A. D. Q.; Yao, J. *Angew. Chem., Int. Ed.* **2011**, *50*, 3715−3719.
(33) Zhang, M.; Meng, L.; Cao, X.; Jiang, M.; Yi, T. *Soft Matter* **2012**, *8*, 4494−4498.
(34) Kume, S.; Kuroiwa, K.; Kimizuka, N. *Chem. Commun.* **2006**, 2442−2444.
(35) Tseng, K.-P.; Tsai, Y.-T.; Wu, C.-C.; Shyue, J.-J.; Bassani, D. M.; Wong, K.-T. *Chem. Commun.* **2013**, *49*, 11536−11538.
(36) Akazawa, M.; Uchida, K.; de Jong, J. J. D.; Areephong, J.; Stuart, M.; Caroli, G.; Browne, W. R.; Feringa, B. L. *Org. Biol. Chem.* **2008**, *6*, 1544−1547.
(37) Zhou, X.; Duan, Y.; Yan, S.; Liu, Z.; Zhang, C.; Yao, L.; Cui, G. *Chem. Commun.* **2011**, *47*, 6876−6878.
(38) Yagai, S.; Ohta, K.; Gushiken, M.; Iwai, K.; Asano, A.; Seki, S.; Kikkawa, Y.; Morimoto, M.; Kitamura, A.; Karatsu, T. *Chem.—Eur. J.* **2012**, *18*, 2244−2253.
(39) Yagai, S.; Iwai, K.; Karatsu, T.; Kitamura, A. *Angew. Chem., Int. Ed.* **2012**, *51*, 9679−9683.
(40) Patra, A.; Métivier, R.; Brisset, F.; Nakatani, K. *Chem. Commun.* **2012**, *48*, 2489−2491.
(41) Yagai, S.; Ishiwatari, K.; Lin, X.; Karatsu, T.; Kitamura, A.; Uemura, S. *Chem.—Eur. J.* **2013**, *19*, 6971−6975.
(42) Zhang, J.; Jin, J.; Zou, L.; Tian, H. *Chem. Commun.* **2013**, *49*, 9926−9928.
(43) van Herpt, J. T.; Areephong, J.; Stuart, M. C. A.; Browne, W. R.; Feringa, B. L. *Chem.—Eur. J.* **2014**, *20*, 1737−1742.
(44) Hirose, T.; Matsuda, K.; Irie, M. *J. Org. Chem.* **2006**, *71*, 7499−7508.
(45) Hirose, T.; Irie, M.; Matsuda, K. *Adv. Mater.* **2008**, *20*, 2137−2141.
(46) Oana, H.; Kishimura, A.; Yonehara, K.; Yamasaki, Y.; Washizu, M.; Kataoka, K. *Angew. Chem., Int. Ed.* **2009**, *48*, 4613−4616.
(47) Pashuck, E. T.; Stupp, S. I. *J. Am. Chem. Soc.* **2010**, *132*, 8819−8821.
(48) Kurihara, K.; Tamura, M.; Shohda, K.-i.; Toyota, T.; Suzuki, K.; Sugawara, T. *Nat. Chem.* **2011**, *3*, 775−781.
(49) Anraku, Y.; Kishimura, A.; Yamasaki, Y.; Kataoka, K. *J. Am. Chem. Soc.* **2013**, *135*, 1423−1429.
(50) Ortony, J. H.; Newcomb, C. J.; Matson, J. B.; Palmer, L. C.; Doan, P. E.; Hoffman, B. M.; Stupp, S. I. *Nat. Mater.* **2014**, *13*, 812−816.
(51) Finkelmann, H.; Nishikawa, E.; Pereira, G. G.; Warner, M. *Phys. Rev. Lett.* **2001**, *87*, 015501.
(52) Yu, Y.; Nakano, M.; Ikeda, T. *Nature* **2003**, *425*, 145.
(53) Yamada, M.; Kondo, M.; Mamiya, J.-i.; Yu, Y.; Kinoshita, M.; Barrett, C. J.; Ikeda, T. *Angew. Chem., Int. Ed.* **2008**, *47*, 4986−4988.
(54) Hamada, T.; Sugimoto, R.; Vestergaard, M. C.; Nagasaki, T.; Takagi, M. *J. Am. Chem. Soc.* **2010**, *132*, 10528−10532.
(55) Faure, D.; Gravier, J.; Labrot, T.; Desbat, B.; Oda, R.; Bassani, D. M. *Chem. Commun.* **2005**, 1167−1169.
(56) Hosono, N.; Kajitani, T.; Fukushima, T.; Ito, K.; Sasaki, S.; Takata, M.; Aida, T. *Science* **2010**, *330*, 808−811.
(57) Kageyama, Y.; Tanigake, N.; Kurokome, Y.; Iwaki, S.; Takeda, S.; Suzuki, K.; Sugawara, T. *Chem. Commun.* **2013**, *49*, 9386−9388.
(58) Uda, R.; Hiraishi, E.; Ohnishi, R.; Nakahara, Y.; Kimura, K. *Langmuir* **2010**, *26*, 5444−5450.
(59) Coleman, A. C.; Beierle, J. M.; Stuart, M. C. A.; Maciá, B.; Caroli, G.; Mika, J. T.; van Dijken, D. J.; Chen, J.; Browne, W. R.; Feringa, B. L. *Nat. Nanotechnol.* **2011**, *6*, 547−552.
(60) Kobatake, S.; Takami, S.; Muto, H.; Ishikawa, T.; Irie, M. *Nature* **2007**, *446*, 778−781.
(61) Koshima, H.; Takechi, K.; Uchimoto, H.; Shiro, M.; Hashizume, D. *Chem. Commun.* **2011**, *47*, 11423−11425.
(62) Irie, M.; Lifka, T.; Kobatake, S.; Kato, N. *J. Am. Chem. Soc.* **2000**, *122*, 4871−4876.
(63) Irie, M.; Sakemura, K.; Okinaka, M.; Uchida, K. *J. Org. Chem.* **1995**, *60*, 8305−8309.
(64) Saika, T.; Irie, M.; Shimidzu, T. *J. Chem. Soc., Chem. Commun.* **1994**, 2123−2124.
(65) Kamiya, H.; Yanagisawa, S.; Hiroto, S.; Itami, K.; Shinokubo, H. *Org. Lett.* **2011**, *13*, 6394−6397.
(66) Pisula, W.; Kastler, M.; Wasserfallen, D.; Pakula, T.; Müllen, K. *J. Am. Chem. Soc.* **2004**, *126*, 8074−8075.
(67) The absorption band around 600 nm also decreased and shifted upon cooling. The decrease proceeded in two stages: a gradual decrease was observed from 35 to 23 °C, and a subsequent rapid decrease occurred below 23 °C (Supporting Information Figure S8).
(68) Gierschner, J.; Park, S. Y. *J. Mater. Chem. C* **2013**, *1*, 5818−5832.
(69) Yagai, S.; Seki, T.; Karatsu, T.; Kitamura, A.; Würthner, F. *Angew. Chem., Int. Ed.* **2008**, *47*, 3367−3371.
(70) Menger, F. M.; Peresypkin, A. V. *J. Am. Chem. Soc.* **2001**, *123*, 5614−5615.
(71) Imura, T.; Yanagishita, H.; Kitamoto, D. *J. Am. Chem. Soc.* **2004**, *126*, 10804−10805.
(72) Hamley, I. W.; Krysmann, M. J.; Castelletto, V.; Noirez, L. *Adv. Mater.* **2008**, *20*, 4394−4397.
(73) Mezzenga, R.; Meyer, C.; Servais, C.; Romoscanu, A. I.; Sagalowicz, L.; Hayward, R. C. *Langmuir* **2005**, *21*, 3322−3333.
(74) Lee, W. B.; Mezzenga, R.; Fredrickson, G. H. *Phys. Rev. Lett.* **2007**, *99*, 187801.
(75) Wei, P.; Cook, T. R.; Yan, X.; Huang, F.; Stang, P. J. *J. Am. Chem. Soc.* **2014**, *136*, 15497−15500.

DOI: 10.1021/ja512924q
J. Am. Chem. Soc. 2015, 137, 2722−2729